The Heated Condensation Framework. Part II: Climatological Behavior of Convective Initiation and Land–Atmosphere Coupling over the Conterminous United States

AHMED B. TAWFIK* AND PAUL A. DIRMEYER

Center for Ocean–Land–Atmosphere Studies, George Mason University, Fairfax, Virginia

JOSEPH A. SANTANELLO JR.

Hydrological Sciences, NASA Goddard Space Flight Center, Greenbelt, Maryland

(Manuscript received 23 June 2014, in final form 1 May 2015)

ABSTRACT

This is Part II of a two-part study introducing the heated condensation framework (HCF), which quantifies the potential convective state of the atmosphere in terms of land–atmosphere interactions. Part I introduced the full suite of HCF variables and applied them to case studies with observations and models over a single location in the southern Great Plains. It was shown in Part I that the HCF was capable of identifying locally initiated convection and quantifying energetically favorable pathways for initiation. Here, the HCF is applied to the entire conterminous United States and the climatology of convective initiation (CI) in relation to local land–atmosphere coupling (LoCo) is explored for 34 summers (June–August) using the North American Regional Reanalysis (NARR) and observations. NARR is found to be capable of capturing the convective threshold (buoyant mixing potential temperature θ_{BM}) and energy advantage transition (energy advantage potential temperature θ_{adv}) for most of the United States. However, there are compensating biases in the components of moisture q_{mix} and temperature q^*, resulting in low θ_{BM} biases for the wrong reason. The HCF has been used to show that local CI occurred over the Rocky Mountains and the southern Great Plains 35%–65% of the time. Finally, the LoCo process chain has been recast in light of the HCF. Both positive and negative soil moisture–convective feedbacks are possible, with negative feedbacks producing a stronger response in CI likelihood under weak convective inhibition. Positive feedbacks are present but weaker.

1. Introduction

The current work applies the heated condensation framework (HCF), detailed in Tawfik et al. (2015, hereafter Part I), at continental scales in order to evaluate the convective initiation (CI) and the corresponding land–atmosphere coupling from a climatological perspective. Because a study of convective initiation involves a series of complex interactions, evaluation becomes more tractable when the system is dissected into components; in this case, an atmospheric segment and a terrestrial segment. Each segment can then be reduced to process-level interactions. Specifically, Santanello et al. (2011) and Santanello et al. (2013) lay out the steps of this process chain as 1) the impact of soil moisture (SM) changes on surface evaporative fraction (EF); 2) the impact of EF on planetary boundary layer (PBL) evolution; 3) the sensitivity of PBL evolution to the top of PBL entrainment (ENT); 4) the feedback between the top of the PBL and surface energy partitioning (EF_{atm} = PBL-modified EF); and 5) the ability to produce cloud cover and precipitation P (Eq. 1):

$$\frac{d(\mathrm{SM})}{d(\mathrm{EF})}\times\frac{d(\mathrm{EF})}{d(\mathrm{PBL})}\times\frac{d(\mathrm{PBL})}{d(\mathrm{ENT})}\times\frac{d(\mathrm{ENT})}{d(\mathrm{EF_{atm}})}\Rightarrow d(\mathrm{Cloud}/P). \tag{1}$$

Note that this process chain focuses on local land–atmosphere coupling (LoCo), meaning a method is required for identifying which convective events originated locally. Such a method currently does not exist,

* Current affiliation: Climate and Global Dynamics, National Center for Atmospheric Research, Boulder, Colorado.

Corresponding author address: Ahmed Tawfik, Climate and Global Dynamics, National Center for Atmospheric Research, 1850 Table Mesa Drive, Boulder, CO 80305.
E-mail: abtawfik@ucar.edu

DOI: 10.1175/JHM-D-14-0118.1

© 2015 American Meteorological Society

making it difficult to assess the full LoCo process chain. Without this capability, interpreting the contribution of the remaining processes [the terms on the lhs of Eq. (1)] becomes difficult, potentially conflating the magnitude and location of soil moisture–precipitation feedbacks. The HCF attempts to fill this gap by identifying which convective events were triggered locally [the term on the rhs of Eq. (1)].

The terrestrial segment, as represented by the first link in the process chain [the first term on the lhs of Eq. (1)], has been the subject of many studies (e.g., D'Odorico and Porporato 2004; Koster et al. 2009; Dirmeyer 2011; Wei and Dirmeyer 2012; Mei and Wang 2012; Ferguson et al. 2012; Liu et al. 2014). In particular, Dirmeyer (2011) introduced an index that accounts for the variability as well as the sensitivity of soil moisture on surface fluxes. Applying this method to several reanalysis datasets, the traditional Global Land–Atmosphere Coupling Experiment (GLACE; Koster et al. 2006; Guo et al. 2006) "hotspots" were returned, lending some confidence that the terrestrial segment plays an important role in producing this signal. The importance of the soil moisture–surface flux relationship to the overall soil moisture–precipitation coupling signal was further reinforced by Wei and Dirmeyer (2012), who, using back-trajectory analysis, showed that the spatial pattern of soil moisture–precipitation coupling was well correlated to regions with strong soil moisture–evaporative fraction coupling. Following the recommended method of Mei and Wang (2012), Liu et al. (2014) calculated a modified version of the Dirmeyer (2011) metric that is based on peak correlation returned from the probability distribution function of conditional correlation coefficients of soil moisture. They found terrestrial coupling strength to be a strong determining factor of soil moisture–precipitation coupling in several models and the Global Land Data Assimilation System (GLDAS).

The atmospheric segment, encompassing the second through fifth process links [the second to fourth terms on the lhs and the term on the rhs of Eq. (1)], has received less attention because of the complication of attributing potentially nonlocal precipitation and cloud cover to variations in soil moisture and surface fluxes. Despite this difficulty, several studies have shown the importance of the atmospheric background state in promoting or dampening positive soil moisture–precipitation feedbacks (Findell and Eltahir 2003a,b; Koster et al. 2006; Hohenegger et al. 2009; Findell et al. 2011; Taylor et al. 2012; Westra et al. 2012). Findell and Eltahir (2003a,b) introduced the convective triggering potential (CTP) and low-level humidity index (HI_{low}) as a way of quantifying how primed the morning atmosphere is to initiating convection. They found that morning soundings can be categorized into five distinct profiles, some of which were conducive to triggering convection for different soil moisture states. Thresholds for these states have been found to be dependent on geography and the source of data (Ferguson and Wood 2011). Computing the CTP–HI_{low} metrics from the North American Regional Reanalysis (NARR; Mesinger et al. 2006), Aires et al. (2014) used a neural network sensitivity analysis to categorize the relative importance of the terrestrial and atmospheric segments within the context of coupling. They found precipitation frequency over the western half of the United States to be atmospherically controlled, with a gradual transition eastward to a more mixed contribution from EF and low-level humidity. Examining the influence of evapotranspiration (ET) on precipitation using back-trajectory analysis, Wei and Dirmeyer (2012) suggest that while very wet soils that correspond to high ET rates can easily trigger precipitation, changes in large-scale moisture transport is the primary driver of precipitation variability for the eastern United States. This seems to contradict Findell et al. (2011), who highlight this region as supporting a positive soil moisture–precipitation feedback regime; however, the contribution of locally originating convection needs to be separated from nonlocal convection to fully realize these feedback regimes.

This study applies the HCF to observations and NARR first to establish the mean convective state and systematic biases present in NARR related to local convective initiation in section 3. Section 4 then identifies regions where CI most frequently occurs and explores CI interannual variability. The conditions leading to the regional differences in CI are presented in section 5 and the atmospheric segment of the process chain (provided by the HCF variables) is connected to the terrestrial segment. Results from the current work are placed within the context of prior land–atmosphere coupling work in section 6. Section 7 concludes with a summary of results and comments on future applications using the HCF.

2. Data

a. NARR

NARR is a data assimilation product that ingests a suite of atmospheric observations into the NCEP Eta Model and produces 3-hourly output. NARR was designed to improve precipitation timing and location by assimilating the diabatic heating profiles associated with precipitation. Further details regarding NARR can be found in Mesinger et al. (2006). We use NARR vertical profiles of temperature, humidity, geopotential height, and pressure spanning 1979–2012 for summer months only [June–August (JJA)] to calculate HCF

variables. NARR is first compared with observations for 1200 UTC morning soundings to judge its ability in capturing the mean convective state using the HCF. Because few observed vertical profiles are available outside of the typical morning (1200 UTC) and evening (0000 UTC) operational sounding launch hours, the NARR is used exclusively for evaluating the behavior of the convective state for the full diurnal cycle.

b. IGRA

The Integrated Global Radiosonde Archive (IGRA; Durre et al. 2006) is a comprehensive database containing quality-controlled observations of atmospheric profiles of temperature, humidity, pressure, geopotential height, and wind speed and direction for over 1500 sites globally. The best spatial and temporal coverage is found over the North America, Eurasia, and Australia. The current work is focused on the continental United States, where over 75 stations have at least 1350 morning (1200 UTC) soundings available during JJA (e.g., approximately 15 summers) from 1979 to 2012, mirroring the years available for NARR. Only stations with at least 15 summers of observations available during the 1979–2012 period are used to calculate HCF variables from temperature, humidity, pressure, and geopotential height profiles; however, the criterion is relaxed to requiring at least 500 morning soundings for the energy advantage potential temperature θ_{adv} bias analysis because not all days may have energy transitions.

c. ISH data

The Integrated Surface Hourly (ISH) dataset contains hourly measurements of typical meteorological variables, such as surface pressure and temperature retrieved from surface observing stations globally. The ISH combines data streams from the National Climatic Data Center networks, which include National Weather Service stations, and U.S. Navy surface observations. This dataset is quality controlled to remove potentially erroneous spikes that may occur. The ISH contains over 20 000 stations archived globally. For the purposes of the current work, we calculate daily maximum potential temperature θ_{max} only for stations that are collocated with the IGRA soundings observations from 1979 to 2012 (same as NARR). This is possible because soundings are often launched within close proximity to surface observation networks. For a station to be included for analysis, at least 1350 summer days must be available (~15 summers). Additionally, because we are focused on JJA, ISH stations were required to have at least 2 months of data for a year to be counted as a complete summer. Furthermore, each day was required to have at least 20 h of nonmissing data to calculate θ_{max} for a given day. While this greatly reduced the number of stations, these constraints provide a more robust evaluation. Here, ISH data are used solely to calculate θ_{max} that is then used to return the convective likelihood using the probability method outlined in Part I.

TABLE 1. Summary of NARR mean, bias, and RMSE compared to IGRA and ISH observations for select regions shown in Fig. 6.

Variable	Region	NARR mean	Mean bias	RMSE	No. of obs sites
θ_{BM}	SE	308.7	2.9	7.3	7
	SP	315.4	1.4	5.0	8
	NP	312.1	1.5	6.4	5
	SW	322.0	0.4	2.3	5
θ_{adv}	SE	302.9	−0.6	3.3	7
	SP	311.5	0.6	3.7	10
	NP	307.7	0.4	3.5	5
	SW	315.8	0.3	3.1	6
θ_{max}	SE	303.9	−0.6	4.1	4
	SP	313.2	1.8	5.8	8
	NP	308.5	3.0	8.0	4
	SW	319.7	1.1	4.5	4

3. Mean conditions and NARR comparison

Here we describe the mean convective state over the conterminous United States for observations and NARR with the intent of highlighting the ability of NARR to capture observed spatial patterns, providing context for discussing CI and LoCo. The buoyant mixing potential temperature θ_{BM} describes the threshold needed to be reached by the potential temperature at 2-m height θ_{2m} in order to trigger convection, while θ_{adv} identifies the transition from moisture input advantage to boundary layer growth advantage (e.g., transition in the most energetically favorable pathway for achieving convection). Analysis is performed at 1200 UTC because of the ready availability of observed atmospheric soundings. A summary of NARR biases can be found in Table 1 for a few select regions.

The observed summer mean spatial pattern of θ_{BM} is well captured in NARR, showing a west-to-east gradient with larger values over the western half of the United States decreasing eastward (Fig. 1a). The highest biases are found along coastal stations, especially for California and southern Texas (Fig. 1b). This is likely due to the sea-breeze effects that have been shown to produce rapid changes in θ_{BM} in less than 2 h (Tawfik and Dirmeyer 2014). Additionally, NARR generally overestimates θ_{BM} over the entire United States, with the smallest biases occurring over the Rocky Mountains and central plains (Fig. 1b). This is further illustrated in the root-mean-square error (RMSE) pattern shown in

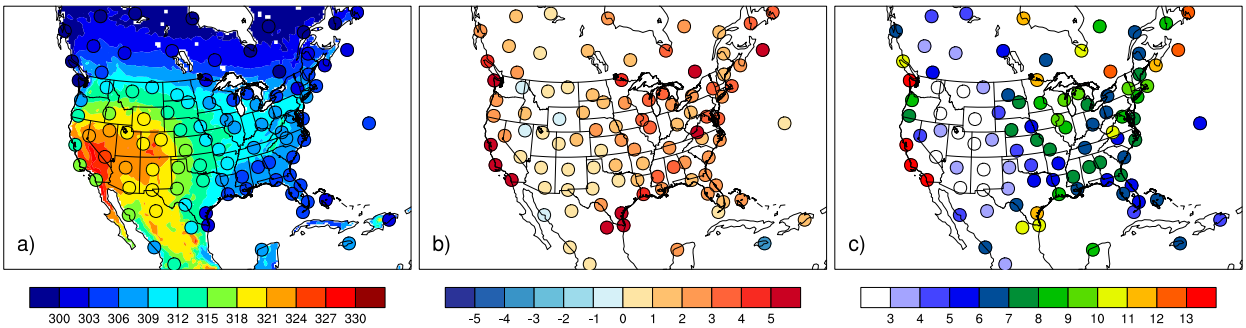

FIG. 1. Summer (a) average, (b) bias (NARR minus observations), and (c) RMSE of θ_{BM} (K) for NARR and IGRA observations at 1200 UTC requiring at least 1350 days of valid data for a station to be included.

Fig. 1c. These low biases over the central plains suggest that θ_{BM} from NARR can provide an accurate representation of the observed convective threshold over the widely recognized land–atmosphere coupling hotspot region (Koster et al. 2006).

The energy advantage potential temperature shows even better agreement compared to observations than θ_{BM}. Similar to θ_{BM}, the maximum θ_{adv} is located over the Southwest and central Rocky Mountains (Fig. 2a). Biases of θ_{adv} are less than 4 K throughout the United States, with a few exceptions along the West Coast, and unlike θ_{BM}, there are no apparent coastal biases in θ_{adv} along the Gulf of Mexico coastline (Fig. 2b). Additionally, RMSE is much lower for θ_{adv}, showing that the energy advantage transition is very well captured in NARR for the entire United States, again with the exception of the Oakland, California, station (Fig. 2c). This shows that while there are slight systematic overestimates in the NARR convective initiation threshold (θ_{BM}), the separation between energetically favorable regimes is well represented.

As described in Part I, to calculate the probability of CI, the probability distribution function of daily maximum potential temperature is used and compared to instances of θ_{BM}. Therefore, biases in θ_{max} are examined to provide insight into any biases found in CI discussed in section 4. As expected, the warmest θ_{max} occurs over the Southwest and central Rocky Mountains, with cooler temperatures toward the east (Fig. 3a). NARR generally appears to overestimate θ_{max}, especially over Southern California (>3 K) and through the Great Plains (Fig. 3b). This warm bias in NARR would likely increase the probability of triggering convection, especially because θ_{BM} biases were low for this region (Fig. 1b). The Southeast shows the lowest biases (Fig. 3b) and lowest RMSE (Fig. 3c); however, the larger θ_{BM} biases (Fig. 1b) could still result in CI probability biases over the Southeast.

We can further understand the cause of θ_{BM} and θ_{adv} biases by dissecting them into their components of moisture q_{mix} and temperature q^* using the HCF. Figures 4a–c shows the average RMSE for each profile below the buoyant condensation level (BCL) (e.g., the average error in each vertical profile for each component) for q_{mix}, q^*, and the specific humidity deficit q_{def} ($=q^* - q_{mix}$). It is evident that the largest errors occur over the Rocky Mountains for q^*, and this translates into higher RMSE for q_{def} (Fig. 4c). This suggests that greater attention should be placed on improving q^* in NARR rather than q_{mix}. However, these biases do not appear to influence θ_{BM} (Fig. 1), suggesting that there may be either some compensating biases in the q_{mix} profile or different sign biases in q^* at various levels.

To better interpret the RMSE, a vertical cross section is taken along a latitudinally averaged band from 33° to 43°N (averaging area shown in Fig. 4c). The q_{mix} in NARR is well captured near the surface across the United States, showing biases less than 2 g kg^{-1} and less than 0.5 g kg^{-1} west of 95°W (Fig. 4d). However, there are large overestimates (>2 g kg^{-1}) above 700 hPa east of the Rocky Mountains. The q^* in NARR shows the greatest biases immediately near the surface, generally overestimating q^* by 1–4 g kg^{-1} east of the Rockies (Fig. 4e). This implies a stronger surface inversion in NARR compared to observations, similar to the two case study days found in Part I. NARR q^* shows low average biases above 100 hPa from the ground. These biases in q_{mix} and q^* translate into positive q_{def} biases near the surface and negative q_{def} biases aloft (Fig. 4f).

This demonstrates that there are compensating biases in NARR, where a stronger surface inversion tends to increase θ_{BM} while more moist conditions aloft tend to decrease θ_{BM}, translating into θ_{BM} biases of less than 4 K (Fig. 1b), despite moisture and temperature biases throughout the atmospheric column. Because CI is only concerned with θ_{BM}, NARR can still serve as a good surrogate for observed convective thresholds where data

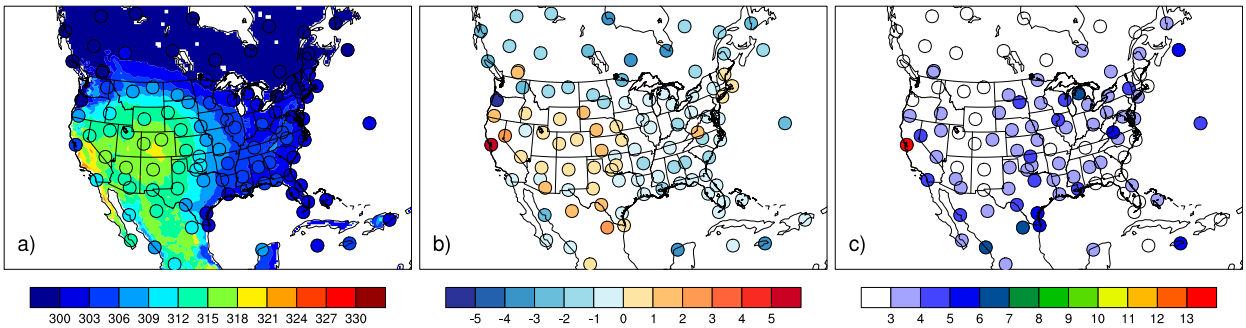

FIG. 2. Summer (a) average, (b) bias (NARR minus observations), and (c) RMSE of θ_{adv} (K) for NARR and IGRA observations at 1200 UTC requiring at least 500 days of valid data for a station to be included.

are not available. The inherent biases in q_{mix} and q^* should be kept in mind, however, when attempting to assess the reasons for changes in the convective threshold. The implications of these biases on CI and land–atmosphere coupling are discussed further in section 6b.

4. Local convective initiation patterns and variability

a. Spatial patterns

To evaluate local CI, the two methods outlined in Part I are applied; the retrospective method and the probability method. While the retrospective method is the most accurate because it is simply a count of the convective threshold being reached (e.g., potential temperature deficit $\theta_{def} = 0$), the retrospective method requires a robust time series of atmospheric profiles throughout the entire diurnal cycle, making comparison with observations difficult outside of the typical sounding launch times, 1200 and 0000 UTC.

Figure 5 shows the frequency of CI for midday and afternoon hours (1800, 2100, and 0000 UTC) using the retrospective method. The Rocky Mountains south of 45°N through central Mexico show the highest occurrences with CI of 35%–65% at 1800 UTC and greater than 55% of the time by 2100 UTC, according to NARR (Figs. 5a,b). Convection is also triggered 25%–45% of the time over the Appalachian Mountains and Florida at 1800 UTC and decreases as the day progresses (Fig. 5). Interestingly, the traditional land–atmosphere coupling hotspot over the central Great Plains does not have high local convective initiation at 2100 UTC (5%–35%), with the exception of Texas (35%–55%). It should be noted, however, that this local coupling diagnostic does not distinguish between shallow and deep convection. This means the higher probability regions may trigger convection that propagates, as is often the case over the plains where convection originates on the lee side of Rockies and moves eastward because of convective organization (Fritsch et al. 1986; Ashley et al. 2003; Moncrieff et al. 2012).

By 0000 UTC the boundary layer begins to collapse over the eastern half of the United States, corresponding to very low occurrences of CI (<5%) in both NARR and observations (Fig. 5c). Additionally, NARR appears to trigger convection 10%–30% more frequently than observed at 0000 UTC over the Rocky Mountains. This discrepancy should be interpreted with caution, however, because being a 3-hourly averaged product, the 0000 UTC NARR sounding likely smooths the sharp transition associated with a collapsing boundary layer. Additionally, the discrepancy may be associated with the warmer θ_{max} found in NARR over the plains (Figs. 3b,c) that could then produce a greater occurrence of convective initiation even when θ_{BM} biases are relatively low for this region (Figs. 1b).

The probabilistic approach has the advantage of avoiding sharp changes in the boundary layer because it compares θ_{BM}, which is not sensitive to boundary layer height changes, against the distribution of daily maximum θ_{max} to assess the likelihood of CI. In agreement with the retrospective approach, the probabilistic approach suggests that the Rocky Mountains have the highest chance of triggering convection (Fig. 6a). The Southeast also shows relatively high probabilities (30%–50%) of triggering convection. Overall, biases show that NARR tends to underpredict CI probabilities over the Southeast (CI is 5%–25% less likely in NARR) and slightly overpredict over the western United States. The highest biases occur along the Florida and Texas coastlines, with greater than 35% underprediction of CI in NARR (Fig. 6b). This is expected considering the rapid changes in θ_{BM} that can occur because of land–seabreeze influences at 1200 UTC (Tawfik and Dirmeyer 2014). On the whole, 75% of U.S. stations have less than 15% bias in CI using the probability method. While the strength of the probability signal is weaker than that of

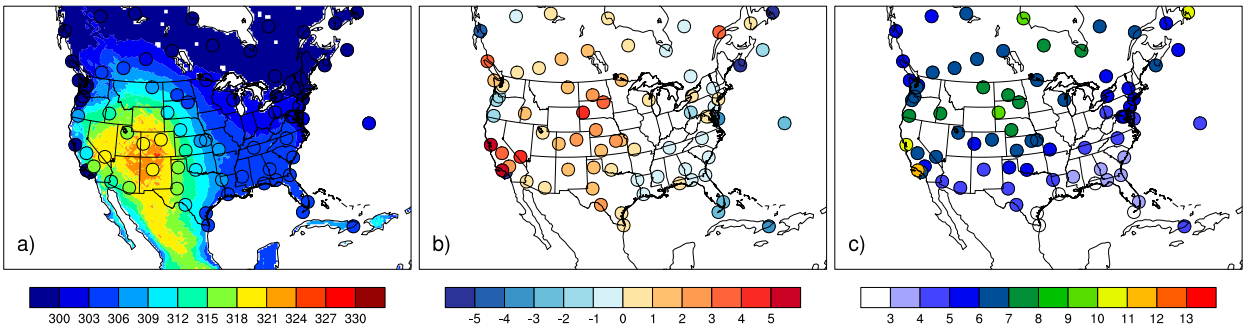

FIG. 3. Summer (a) average, (b) bias (NARR minus observations), and (c) RMSE of θ_{max} (K) for NARR and ISH observations requiring at least 1350 days of valid data for a station to be included.

the retrospective method, it is encouraging that the spatial patterns are consistent.

b. Interannual variability

Interannual variability of CI is explored for both probabilistic and retrospective approaches over a few regions, the Southeast (SE), northern and southern Great Plains (NP and SP), and the Southwest (SW; regions illustrated in Fig. 6b). Note that only the probabilistic approach can be compared against observations at this time. Therefore, it is used to establish the ability of NARR to compare interannual CI changes against observations, providing context for the more accurate retrospective method that is solely applied to NARR.

NARR captures the observed variability well for most regions using the probabilistic approach, especially over the Great Plains and the Southwest, where coefficients of determination R^2 are above 0.74 (Fig. 7). Considering that the comparison is between multiple point observations, whose range is represented by the gray region in Fig. 7, NARR and the observations show remarkably good correspondence. This suggests that only a few soundings are required to provide generally good representation of CI over a relatively large region when using the probabilistic approach. The exception is the Southeast, which returns an R^2 of 0.34. The weak correlation may reflect the relatively high θ_{BM} biases found in this region (Table 1), which would tend to suppress CI in NARR.

Focusing on monthly summer anomalies from a number of CI events using the retrospective method applied to NARR only (Fig. 8), certain years stand out as having lower-than-average CI events. For example, the 2006 and 2007 summers over the SP, NP, and SW regions had at least 1 month with 10 fewer CI events than average (Fig. 8). Prior studies focused over the southern Great Plains note that the 2006 and 2007 summers provide an ideal comparison of anomalously dry (second driest) and wet years (seventh wettest), respectively (Dong et al. 2011; Santanello et al. 2013). In the case of 2007, Dong et al. (2011) showed that the onset of the extremely wet conditions was produced by nonlocal organized mesoscale convective systems propagating eastward, resulting in a largely atmospheric controlled land–atmosphere coupling regime (Santanello et al. 2013). This is consistent with the reduced number of CI events shown for SP in Fig. 8, which resulted from relatively cooler θ_{2m} (JJA average = 305.5 K; 1.2 K cooler than average), making θ_{BM} less attainable. This is in contrast to 2006, which, while having warmer-than-average θ_{2m} (JJA average = 307.6 K; 0.8 K warmer), also had θ_{BM} anomalies that were greater (1.1 K warmer). It is therefore necessary to evaluate the interplay between θ_{2m} and θ_{BM} in order to understand anomalous CI events found in a given year.

Comparing the two methods, we find instances where there is large disagreement. For example, the retrospective method shows anomalously fewer CI events in 2007 for the southern plains (Fig. 8), whereas the probability method returned a slightly above average likelihood of CI (5% increased likelihood; Fig. 7). Because the probability method uses a stationary probability distribution of θ_{max} (i.e., it does not vary from year to year), the anomalously wet soil moisture conditions in 2007 resulting in cooler θ_{max} would not be captured by the probabilistic approach. This results in overestimates of CI likelihood where large interannual variability of θ_{max} is present and points to the importance of the soil moisture state in triggering convection. A bivariate probability distribution of θ_{max} that accounts for soil moisture conditions would likely better constrain the probability method and lead to better correspondence with the retrospective method.

5. Conditions associated with CI

a. Spatial patterns

The energy advantage E_{adv} quantifies the most energetically favorable pathway for initiating convection and can be used to understand the nature of CI. As described

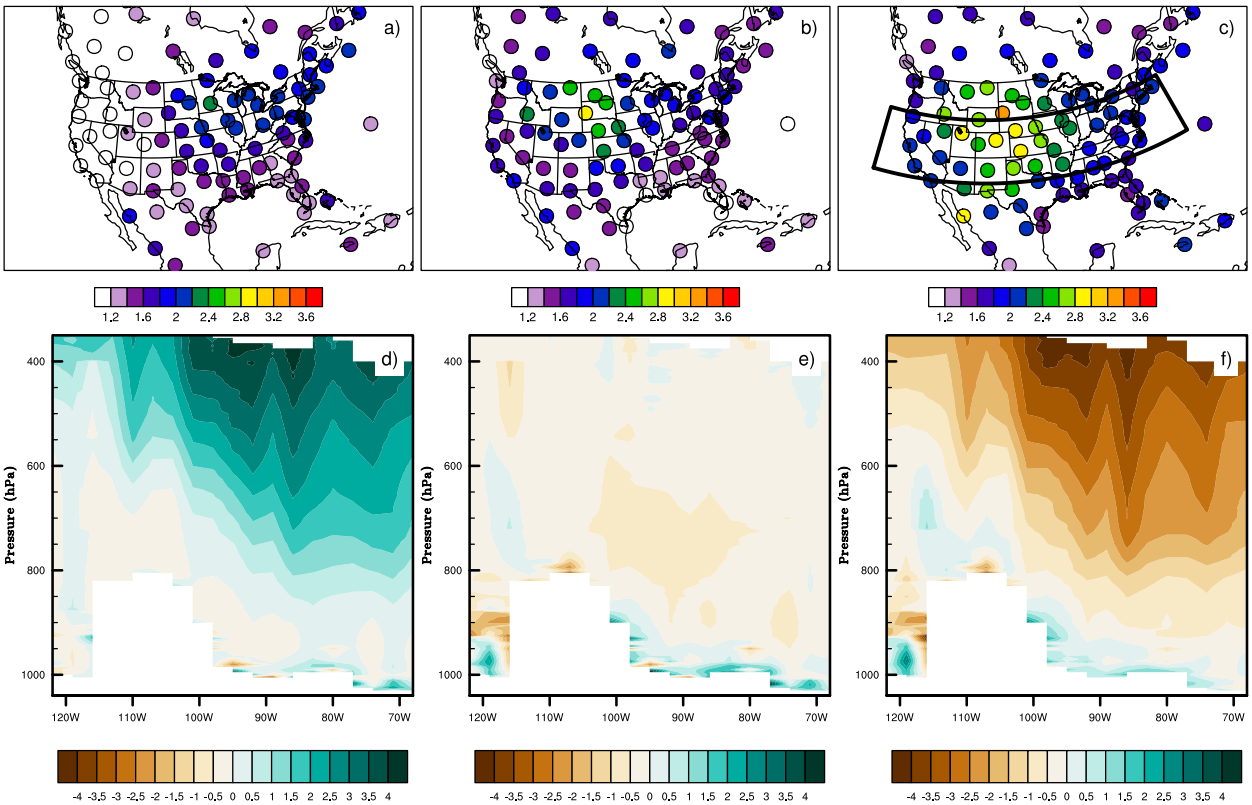

FIG. 4. Summer RMSE of (a) q_{mix}, (b) q^*, and (c) q_{def} profiles below the BCL for NARR and IGRA soundings at 1200 UTC and vertical cross sections of profile biases (NARR minus observations) of (d) q_{mix}, (e) q^*, and (f) q_{def} along the averaging region shown in (c). All units are g kg^{-1}.

in detail in Part I, E_{adv} is constructed from two vector components that describe the additional sensible heat needed to grow the PBL to reach the BCL (SH_{def}; y component) and the additional moisture required to lower the BCL to intersect the PBL (LH_{def}; x component). When E_{adv} is greater than 45°, it is more energetically favorable to grow the boundary layer to reach saturation (referred to as a PBL advantage regime). The converse is true for E_{adv} less than 45°, where adding moisture to the boundary layer is a more expedient route for CI (referred to as a moistening advantage regime).

The average diurnal cycle of E_{adv} is shown in Fig. 9. At 1200 UTC close to sunrise, the entire United States is in a moistening advantage regime (Fig. 9a). This is anticipated because SH_{def} is maximized right before sunrise because of the minimum in θ_{2m}. By 1800 UTC, the southern half of the United States, the Southwest, and the Rockies quickly transition into a PBL advantage regime. Only the Great Lakes region, the West Coast, and parts of the Northeast remain in moistening advantage regimes throughout the day. By the afternoon (2100 UTC; Fig. 9d) and coincident with the PBL height maximum, a distinct PBL advantage ($E_{adv} > 50°$) is established along the lee side of the Rocky Mountains and over most of Florida. This shows that a PBL advantage can be established under dramatically different background climate states, where the lee side of the Rocky Mountains tends to be arid or semiarid and Florida is characterized by a humid, maritime summer climate. The diurnal change in E_{adv} is driven by the growth of the boundary layer. As the depth of the boundary layer increases, a greater amount of absolute moisture is required to reduce the specific humidity deficit at the top of the boundary layer (i.e., q_{def}). Additionally, a growing boundary layer corresponds to a decrease in SH_{def} (due to the PBL height approaching the BCL) and a simultaneous increase in LH_{def} as specific humidity is mixed throughout the PBL. Therefore, increasing the height of the boundary layer generally shifts the energetically favorable pathway for CI from moisture to PBL advantage. For those regions that remain in a moistening advantage, the SH_{def} is much higher, indicating strong convective inhibition.

Within the context of CI there is an apparent correspondence between those regions in a PBL advantage regime and an elevated number of CI events. Focusing

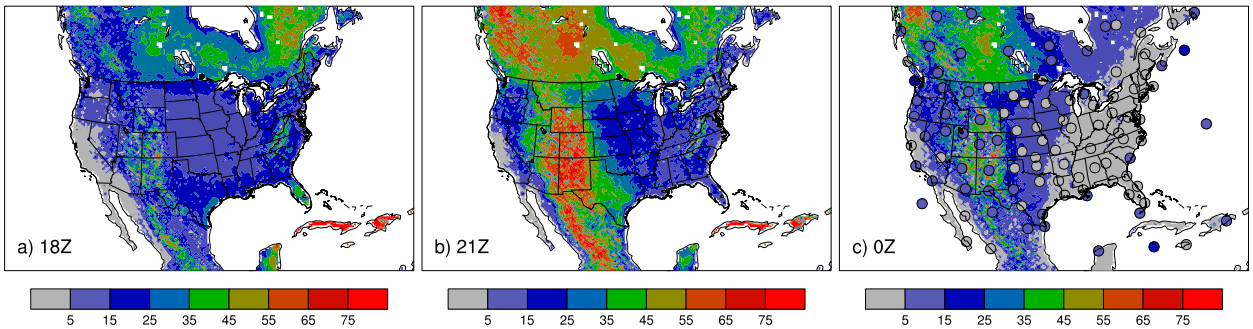

FIG. 5. The percent frequency of local CI at (a) 1800, (b) 2100, and (c) 0000 UTC during JJA using the retrospective method from NARR (contours) and IGRA observations (markers at 0000 UTC).

on the four regions, we find that the SW and SP show strong positive correlations (R = 0.81 for SW and R = 0.68 for SP) between daytime average E_{adv} (1500–0000 UTC) and the number of CI events (Fig. 10a). This suggests that a greater number of CI events occur when there is a PBL advantage for these regions. The number of CI events for the SE and NP, on the other hand, show little relation to changes in E_{adv} (Fig. 10a). In particular, daytime average E_{adv} values for SE and NP largely lie within the moistening advantage regime, with the SE returning the lowest number of CI events and the NP showing a comparable number of CI events to the SP. The comparable number of CI events for the different energy advantage regimes suggests that it is possible to trigger convection through two different mechanisms.

To better understand these different E_{adv} pathways, the number of CI events is also related to the morning (1200 UTC) conditions of θ_{BM} and θ_{2m}. Note that information of these quantities is contained within SH_{def}, and the relationships emerging from θ_{BM} and θ_{2m} represent the daily initial condition of the atmospheric state (i.e., θ_{BM}) and initial the surface-forced state (i.e., θ_{2m}) on CI.

The number of CI events generally increases with decreasing θ_{BM}, as is anticipated with a reduction in the threshold for triggering convection (Fig. 10b). The obvious exception is the SE region, which shows weak θ_{BM} and CI variability, resulting in no obvious relationship. There is clear banding, however, among the four regions where the driest climate, the SW, tends to have a larger range in θ_{BM} and a higher number of CI events. This range is reduced when compared to the wettest region, the SE (Fig. 10b). The average morning θ_{2m} also returns four distinct relationships with CI (Fig. 10c). The SW region shows a positive relationship between CI and θ_{2m} (e.g., warmer morning surface temperatures correspond to more CI). The NP region returns the opposite relationship, suggesting more CI events occur when morning temperatures are cooler. The SP and SE show little variability in θ_{2m} and hence no discernable relationship with CI (Fig. 10c). It should be noted, however, that the ranges in θ_{2m} are smaller relative to those found for θ_{BM}. Taking θ_{BM} and θ_{2m} together as quantified by θ_{def}, the SW, SP, and NP regions overlap and return a negative correlation with CI (Fig. 10d), meaning higher deficits (e.g., higher convective inhibition) correspond to a reduced likelihood of triggering convection. The number of CI events over the SE does not exhibit any sensitivity to morning θ_{def}, suggesting that other factors limit convective initiation for this region.

b. *Local land–atmosphere coupling and the HCF*

Given that the HCF allows for the separation of the initial atmospheric state through θ_{def} and the identification of which convective events were triggered locally, we can recast the LoCo soil moisture–precipitation process chain [described by Eq. (1)] in the context of the HCF [Eq. (2)]. The recasting is performed to remove the ambiguous PBL term found in Eq. (1) and replaces it with a quantifiable HCF variable (i.e., θ_{def}) that pertains directly to local convective initiation. Using the HCF, we can then consider the process chain in terms of convective initiation as

$$\frac{d(\mathrm{CI})}{d(\mathrm{SM})} = \frac{d(\mathrm{EF})}{d(\mathrm{SM})} \times \frac{d(\theta_{2m})}{d(\mathrm{EF})} \times \frac{d(\theta_{def})}{d(\theta_{2m})} \times \frac{d(\mathrm{CI})}{d(\theta_{def})}. \quad (2)$$

Here, SM is volumetric soil moisture ($m^3\,m^{-3}$) and EF is the evaporative fraction. Because CI is a discrete condition of θ_{def} (e.g., when $\theta_{def} = 0$), the last derivative on the right-hand side of Eq. (2) may not be described as a continuous derivative. We can, however, collapse the remaining derivatives on the right-hand side of the equation and examine the changes in the number of monthly total CI events as a function of θ_{def} and 0–10-cm soil moisture (Fig. 11a). There appears to be a clear increase in the number of CI events in a given summer month for drier soils with a small θ_{def} (Fig. 11a).

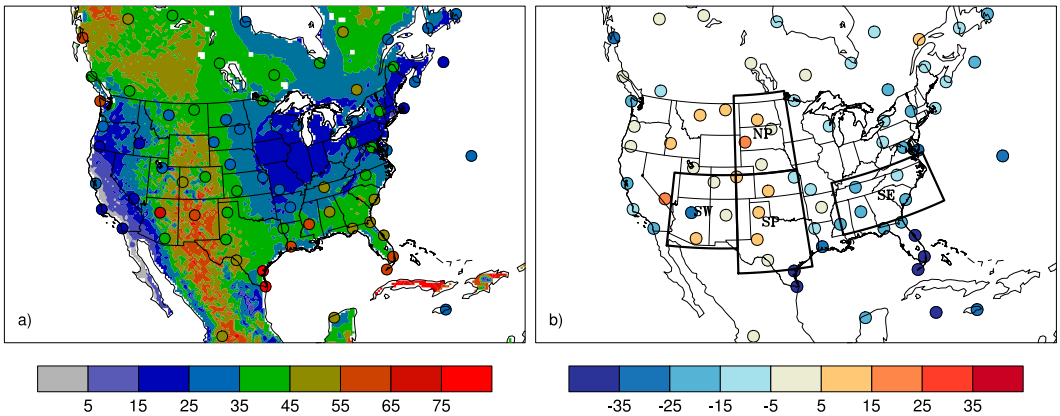

FIG. 6. (a) The percent likelihood of local CI using the probability method at 1200 UTC. (b) The bias (NARR minus observations) in CI probability at 1200 UTC. Regions in (b) identify averaging domains used in Table 1 and subsequent figures.

Additionally, well-correlated lines of constant CI seem to emerge. For example, months that have between 5 and 12 CI events have an R of -0.77 and a slope of $-54\,\mathrm{K\,m^{-3}\,m^{-3}}$, meaning the number of CI events would show little change if a $0.09\,\mathrm{m^3\,m^{-3}}$ increase in soil moisture were accompanied by a 5-K reduction in θ_{def}. Soil moisture and θ_{def} become less correlated for higher CI events, however ($R = -0.46$ for CI events greater than 40).

Beyond these four regions, the probability of triggering convection for all days (92 days $\times$ 34 years) at all NARR grid cells over the United States can be evaluated as a function of θ_{def} and soil moisture (Fig. 11b). This avoids the issue of the discrete nature CI and quantifies how daytime CI (1500–0000 UTC) changes in response to variations in morning (1200 UTC) 0–10-cm soil moisture and morning θ_{def}. We find that the highest probabilities (>65%) for CI occur when the morning θ_{def} is below 10 K and surface soil moisture is drier than $0.2\,\mathrm{m^3\,m^{-3}}$ (Fig. 11b). However, the likelihood of CI drops rapidly from 65% to less than 15% when θ_{def} is increased by 10 K for drier morning soils. This shows convective initiation is most sensitive to the atmospheric background state when soils are drier than $0.2\,\mathrm{m^3\,m^{-3}}$ and points to an atmospherically controlled regime. This result is in agreement with several studies that highlight the Southwest as atmospherically controlled (Findell and Eltahir 2003b; Aires et al. 2014; Berg et al. 2013). It should be noted, however, that these studies used evaporative fraction rather than soil moisture to isolate the atmospheric segment.

For intermediate soil moisture ranges (0.2–$0.3\,\mathrm{m^3\,m^{-3}}$), we find wetter soils actually reduce the likelihood of triggering convection contingent on the atmosphere being relatively close to convection ($\theta_{\mathrm{def}} < 15\,\mathrm{K}$). Specifically, at a constant θ_{def} equal to 10 K, the probability of triggering convection is reduced by 20% for wetter soils within the intermediate soil moisture range (Fig. 11b). This suggests that while the atmosphere may be relatively moist and near convection, wetter soils tend to inhibit boundary layer growth and reduce the ability for the BCL to be reached. Interestingly, within the intermediate soil moisture range the likelihood of CI is less responsive to changes in θ_{def} when compared to the drier soil moisture range. This emphasizes a shift in the sensitivity of CI toward less atmospheric control and an increasing influence from the land surface.

The weakest change in CI likelihood is found when morning soils are within the wettest range ($>0.3\,\mathrm{m^3\,m^{-3}}$; Fig. 11b). Specifically, for weak convective inhibition (θ_{def} approximately equal to 10 K) the probability of CI is low (15%–35%) relative to drier soils reaching a minimum likelihood between 15% and 25%. Under wetter soils, there is a weak reduction in CI frequency when increasing θ_{def}, resulting in a 5%–25% chance of triggering convection when θ_{def} is greater than 15 K and a 5%–15% chance for θ_{def} as high as 50 K. The likelihood of CI appears to rebound at very wet soil moisture ranges ($>0.42\,\mathrm{m^3\,m^{-3}}$) and also corresponds to a reduction in CI at higher θ_{def}. It is currently unclear what may be producing this rebound in CI probability.

6. Discussion

a. Physical mechanism and feedbacks

The physical processes underlying the CI probability changes are in line with those described in previous studies (Ek and Holtslag 2004; van Heerwaarden et al. 2009; Seneviratne et al. 2010; Santanello et al. 2013). In

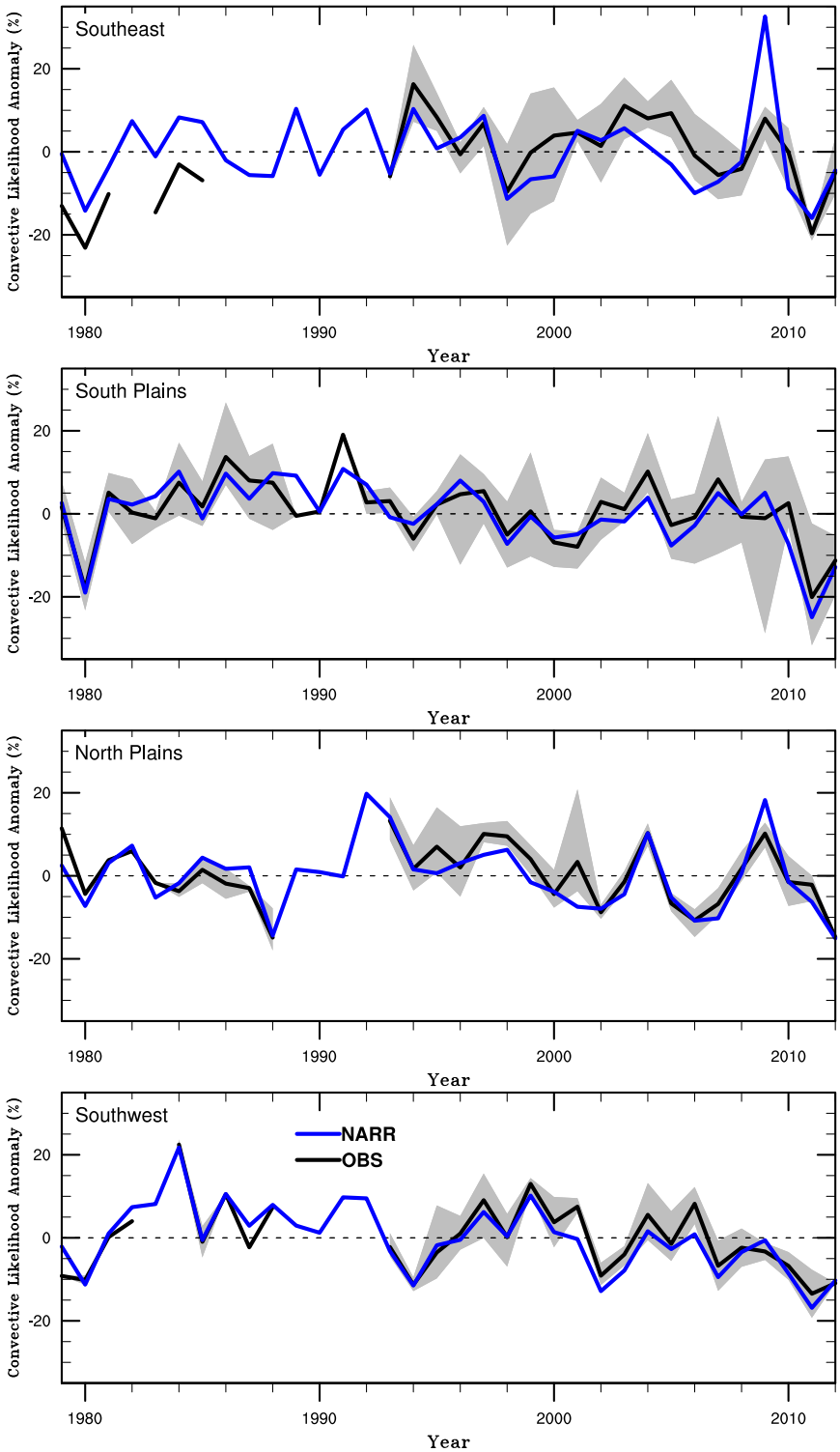

FIG. 7. Anomalies of summer average likelihood of triggering convection using the probability method for the four averaging regions shown in Fig. 6. NARR is shown in blue and observations are in black. The gray shaded region shows the spread in observed stations.

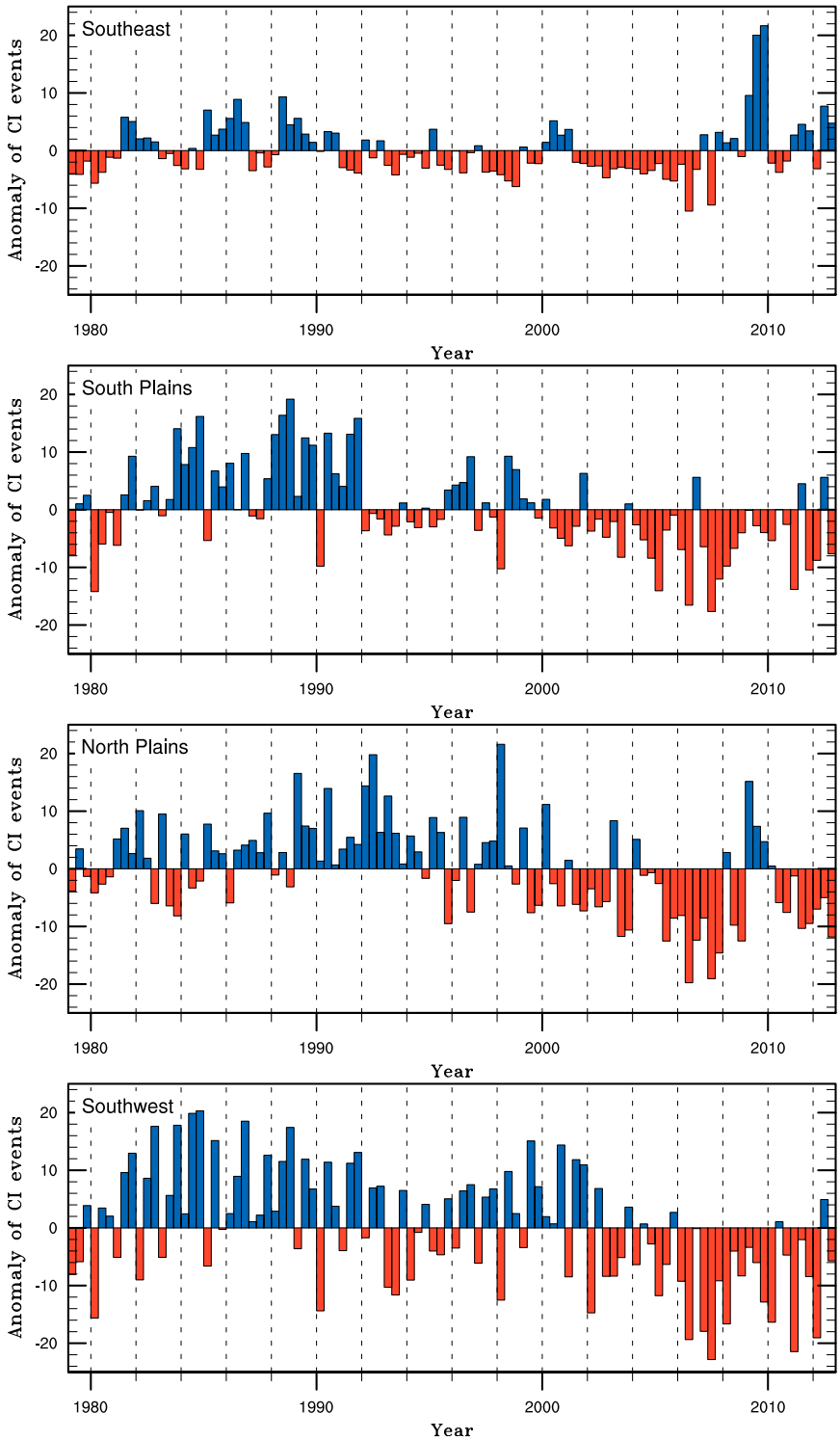

FIG. 8. Anomalies of the number of local CI events for each summer month using the retrospective method for the four averaging regions shown in Fig. 6 calculated from NARR. Positive (negative) anomalies shown in blue (red) indicate more (fewer) CI events for a given summer month.

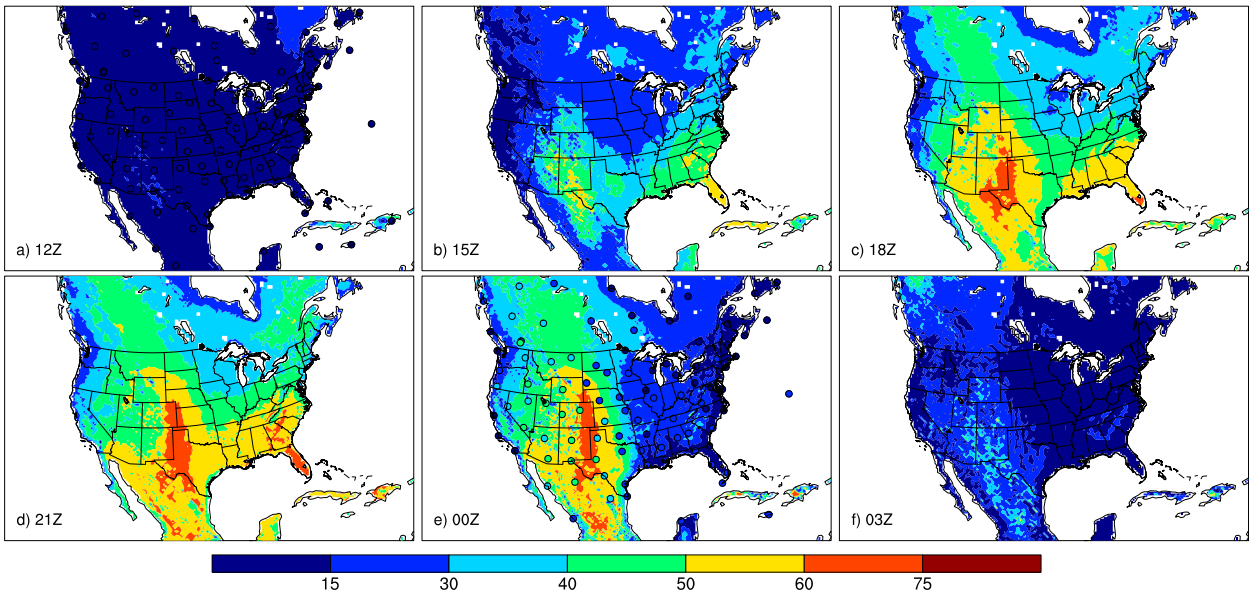

FIG. 9. Summer average diurnal cycle of E_{adv} (°) from 1200 to 0300 UTC. Contours are from NARR and markers are from IGRA soundings only at 0000 UTC.

particular, there have been asymmetric responses to soil moisture and evaporative fraction found in both the terrestrial (Koster et al. 2009; Seneviratne et al. 2010) and atmospheric (Ek and Holtslag 2004; van Heerwaarden et al. 2009; Gentine et al. 2013) segments. The terrestrial asymmetry is produced because a particular region lies on differing ends of the soil moisture– to energy-limited spectrum producing different responses when the soil is dried or moistened. The atmospheric asymmetry is more subtle and involves the balance between surface heating, boundary layer growth, and free troposphere humidity (Betts 2009; van Heerwaarden et al. 2009; Gentine et al. 2013). We find this atmospheric asymmetry in the rapid reduction of convective initiation probability at drier soils versus the more gradual reduction at wetter soils (Fig. 11b). The process underlying this asymmetry in the atmosphere likely follows from the sensitivity of θ_{2m} to soil moisture through the evaporative fraction [first two derivatives in Eq. (2)]. Specifically, surface energy would be mainly partitioned toward sensible heat flux under very dry soils resulting in warmer θ_{2m} and generally higher PBL heights. Because there is a weak source of moisture from the surface coincident with a deep boundary layer, the morning atmosphere must be preconditioned with a sufficient amount of moisture in order for saturation to occur. This results in a strongly atmospherically controlled regime at the driest soil moisture ranges (Fig. 11b) and is in agreement with several studies that point to the western United States (Findell and Eltahir 2003b; Findell et al. 2011; Berg et al. 2013; Aires et al. 2014) and southern Great Plains (Ruiz-Barradas and Nigam 2013) as atmospherically controlled, as well as those studies that suggest the presence of a negative soil moisture–precipitation regime (Juang et al. 2007; Hohenegger et al. 2009; Taylor et al. 2012; Westra et al. 2012; Gentine et al. 2013).

As the soil surface becomes wetter, surface energy fluxes are partitioned more toward evaporation and result in cooler θ_{2m} dampening the diurnal temperature range (Betts and Ball 1995). This acts to restrain boundary layer growth and shifts the limiting step for convective initiation away from the atmosphere and toward increasing θ_{2m} to meet θ_{BM} (the trigger threshold). The shift in behavior is represented by the reduced likelihood of triggering convection for wetter soils when the overlying atmosphere is characterized by weak convective inhibition (Fig. 11b). However, convection may be triggered under conditions of strong convective inhibition with shallow boundary layers through the accumulation of moisture from surface evaporation. This reflects a positive feedback and is in agreement with those studies that show a strong inversion is needed to accumulate moisture from surface evaporation (Ek and Holtslag 2004; Huang and Margulis 2011; Gentine et al. 2013). This feature is highlighted in Fig. 11b through the extension of convective triggering probabilities greater than 5% under strong morning convective inhibition. The positive feedback signal is weaker than that shown for the negative feedbacks, however.

The implication is that both positive and negative soil moisture–precipitation feedbacks can occur depending on where in the θ_{def}–soil moisture domain a particular

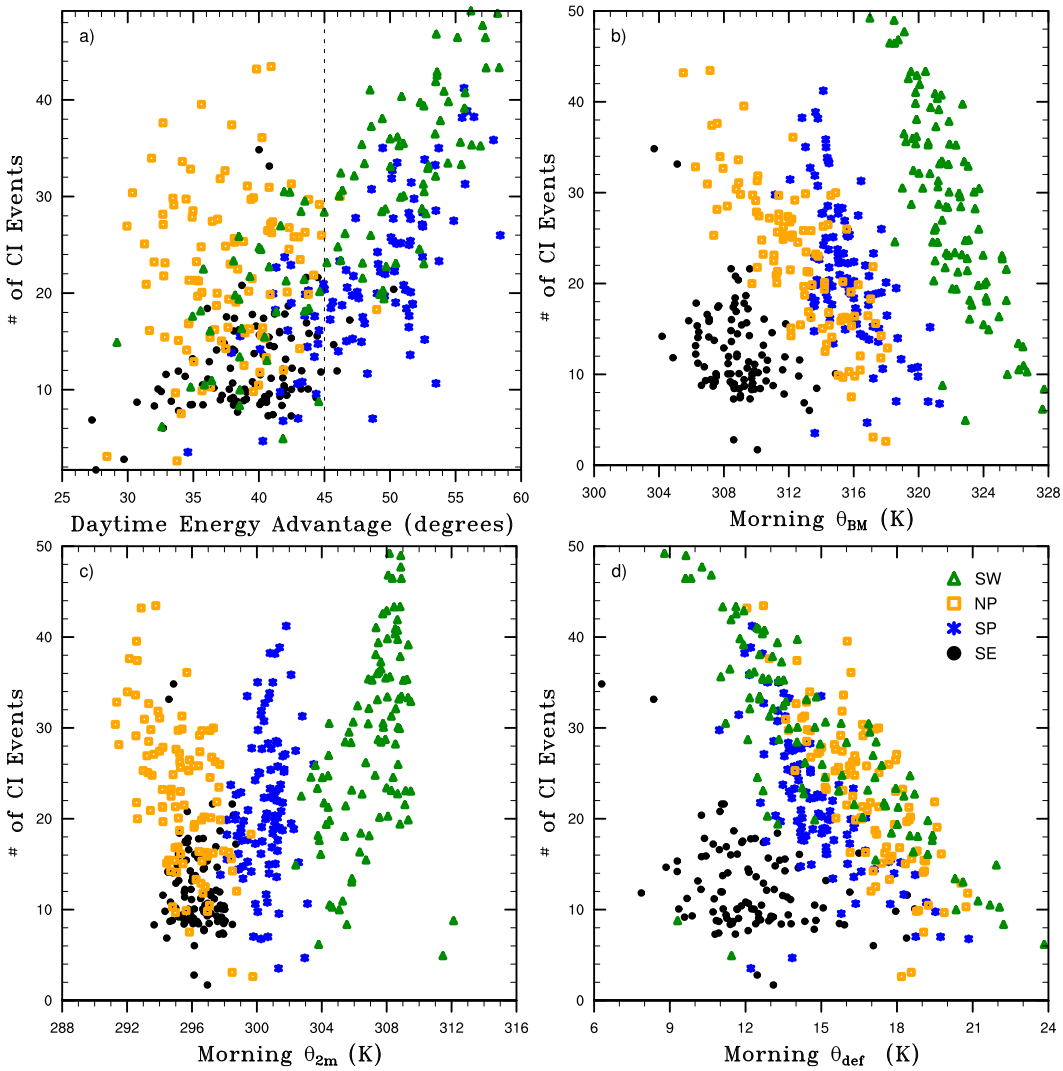

FIG. 10. Comparison of the number of summer monthly local CI events with (a) daytime average (1200–0300 UTC) E_{adv}, (b) morning average (1200 UTC) θ_{BM}, (c) morning average θ_{2m}, and (d) morning average θ_{def} for the SE (black), SP (blue), NP (orange), and SW (green) regions derived from NARR. Vertical line in (a) defines the separation between the moistening advantage (<45°) and the PBL growth advantage (>45°) regimes.

location is found (Fig. 11b). Therefore, although there have been seemingly contradictory results as to the sign and location of soil–precipitation feedbacks (e.g., Guo et al. 2006; Hohenegger et al. 2009; Findell et al. 2011; Ferguson et al. 2012; Taylor et al. 2012, 2013; Berg et al. 2013), this may be the result of 1) model dependence of results, as was highlighted during GLACE-1 (Koster et al. 2006; Guo et al. 2006; Dirmeyer et al. 2006), and 2) narrow focus on specific regions or times that do not encompass a wide enough climate range, thereby limiting interpretation. By separating out the atmospheric segment and identifying local convective initiation events using the HCF, the relative contributions of the land and atmosphere can be disentangled for both models and observations to help determine what regimes are best represented.

b. Limitations

While the absolute mean biases in threshold variables found in NARR were small in most regions (Table 1), the particular moisture and heat components returned compensating errors, producing the low biases in the convective threshold (Fig. 4). Because the calculation of CI relies solely on θ_{BM} and θ_{2m}, the issue of compensating errors would not be expressed in the analysis of CI spatial and regional behavior (sections 4 and 5a), except in those regions with high biases, such as coastal areas and the southeastern United States. The overestimates

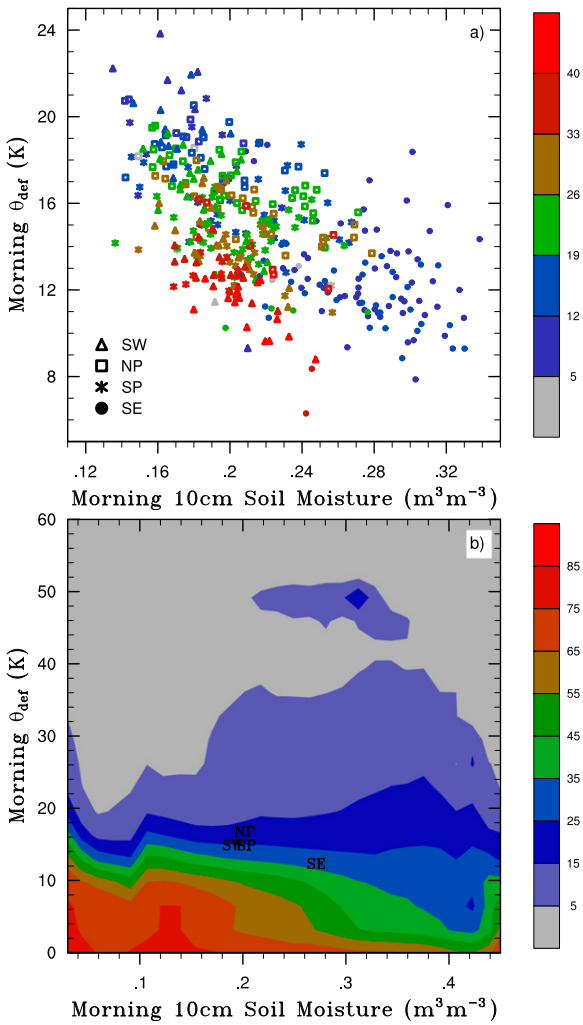

FIG. 11. (a) Comparison of the morning average (1200 UTC) θ_{def} and morning average 10-cm soil moisture colored by the number of local CI events in a given month. (b) The percent probability of triggering convection as a function of θ_{def} and 10-cm soil moisture derived from 34 years of daily NARR summer data. The four averaging regions are overlaid for context.

in θ_{BM} suggest that NARR would have fewer CI events than observed and weaker correlations when compared to observed soundings despite the assimilation of the same soundings. This manifests in a CI correlation coefficient of 0.34 over the Southeast region compared to an R^2 greater than 0.74 for the remaining regions (illustrated in Fig. 7). It has also been noted that NARR tends to overestimate evapotranspiration rates, potentially leading to drier soils than observed, especially during the spring and summer (Nigam and Ruiz-Barradas 2006). These evapotranspiration biases may then influence the CI probabilities that were presented in sections 5b and 5c by overpopulating the dry soil moisture regime and shifting the CI probability maximum (Fig. 10b). However, there are compensating effects of a dry soil moisture bias and a higher-than-observed convective threshold (i.e., θ_{BM}) on CI probability when taken together. This is because drier soils would tend to increase θ_{2m} and thus lead to more CI events, while higher θ_{BM} would tend to suppress CI.

Another issue that arises is the horizontal resolution of NARR. While this is certainly a unique high-resolution reanalysis product, 32 × 32 km grid cells may underpredict CI by averaging over subgrid θ_{2m} maxima that would otherwise reach the θ_{BM} (as can be the case for fair weather cumulus). The 3-hourly temporal resolution may also lead to reductions in the number of CI events by smoothing the daily temperature maximum. The next step is to apply the HCF more broadly to first assess the nature of CI in high-temporal-resolution in situ and remotely sensed observations, and then to validate the nature of LoCo found in models.

7. Summary and conclusions

The climatological behavior and nature of convective initiation has been explored using 34 years of summer data from NARR over the continental United States. It has been shown that, despite capturing the convective threshold and energy transition well in some regions (e.g., the Rocky Mountains and Great Plains), NARR's morning near-surface inversion and free troposphere mixed humidity (i.e., q_{mix}) were generally overestimated, producing compensating errors. This does not influence the calculation of convective initiation events because there are still low biases in the convective threshold. The HCF is also able to identify which convective events were locally triggered, capturing the reduction in convective initiation events during drought months and those months with significant contributions from nonlocally convective initiation. The Southwest and Rocky Mountains are shown to have the highest occurrence of convective initiation with a maximum at 2100 UTC. Recasting the process-chain interactions in terms of the HCF and separating the atmospheric segment from the terrestrial reveals that both positive and negative soil moisture–convection feedbacks are possible. While drier soils tend to trigger convection more frequently, they are also highly sensitive to the atmospheric state. The atmospheric sensitivity is reduced for wetter morning soil moisture conditions, but the change in convective triggering probability is weak relative to the drier soil regime. It should be noted, however, that this method currently does not distinguish between precipitating and nonprecipitating convection and additional metrics are currently being developed to make this distinction.

By having a direct tool for quantifying the atmospheric segment requiring only temperature and humidity profiles, the HCF can be applied to both observational data and model output. While the focus here is on understanding the behavior of convective initiation and introducing a method for quantifying the atmospheric segment of LoCo, the sensitivity of convective initiation to morning soil moisture and convective inhibition can be used ultimately to improve forecast lead times. This would be possible through improving model initialization of soil moisture and evapotranspiration for those regions especially sensitive to the land surface state, as was highlighted by the second phase of GLACE (Koster et al. 2011; Guo et al. 2011). Beyond modeling efforts, regular measurements of soil moisture coincident with the operational radiosonde networks could facilitate real-time evaluation of land–atmosphere coupling by exploiting current techniques like the HCF and mixing diagrams (Santanello et al. 2013) and exploiting the θ_{def}–soil moisture relationship presented here. Until such a broad observational dataset is populated, we will have to rely on reanalysis and remotely sensed data to evaluate the nature of convective initiation and land–atmosphere coupling, which can then be used to confront models. Future work will focus on applying the HCF and CI analysis globally, enabling a broader context for understanding LoCo processes.

Acknowledgments. This work was supported by National Science Foundation Grant 0947837 for Earth System Modeling postdocs. We thank Chiel van Heerwaarden for his excellent review and feedback regarding the methodology and Craig Ferguson for the early discussion that aided in the development of a portion of this work.

REFERENCES

Aires, F., P. Gentine, K. L. Findell, B. R. Lintner, and C. Kerr, 2014: Neural network–based sensitivity analysis of summertime convection over the continental United States. *J. Climate*, **27**, 1958–1979, doi:10.1175/JCLI-D-13-00161.1.

Ashley, W. S., T. L. Mote, P. G. Dixon, S. L. Trotter, E. J. Powell, J. D. Durkee, and A. J. Grundstein, 2003: Distribution of mesoscale convective complex rainfall in the United States. *Mon. Wea. Rev.*, **131**, 3003–3017, doi:10.1175/1520-0493(2003)131<3003:DOMCCR>2.0.CO;2.

Berg, A., K. Findell, B. R. Lintner, P. Gentine, and C. Kerr, 2013: Precipitation sensitivity to surface heat fluxes over North America in reanalysis and model data. *J. Hydrometeor.*, **14**, 722–743, doi:10.1175/JHM-D-12-0111.1.

Betts, A. K., 2009: Land-surface–atmosphere coupling in observations and models. *J. Adv. Model. Earth Syst.*, **2**, doi:10.3894/JAMES.2009.1.4.

——, and J. H. Ball, 1995: The FIFE surface diurnal cycle climate. *J. Geophys. Res.*, **100**, 25 679–25 693, doi:10.1029/94JD03121.

Dirmeyer, P. A., 2011: The terrestrial segment of soil moisture–climate coupling. *Geophys. Res. Lett.*, **38**, L16702, doi:10.1029/2011GL048268.

——, R. D. Koster, and Z. Guo, 2006: Do global models properly represent the feedback between land and atmosphere? *J. Hydrometeor.*, **7**, 1177–1198, doi:10.1175/JHM532.1.

D'Odorico, P., and A. Porporato, 2004: Preferential states in soil moisture and climate dynamics. *Proc. Natl. Acad. Sci. USA*, **101**, 8848–8851, doi:10.1073/pnas.0401428101.

Dong, X., and Coauthors, 2011: Investigation of the 2006 drought and 2007 flood extremes at the southern Great Plains through an integrative analysis of observations. *J. Geophys. Res.*, **116**, D03204, doi:10.1029/2010JD014776.

Durre, I., R. S. Vose, and D. B. Wuertz, 2006: Overview of the integrated global radiosonde archive. *J. Climate*, **19**, 53–68, doi:10.1175/JCLI3594.1.

Ek, M. B., and A. M. Holtslag, 2004: Influence of soil moisture on boundary layer cloud development. *J. Hydrometeor.*, **5**, 86–99, doi:10.1175/1525-7541(2004)005<0086:IOSMOB>2.0.CO;2.

Ferguson, C. R., and E. F. Wood, 2011: Observed land–atmosphere coupling from satellite remote sensing and reanalysis. *J. Hydrometeor.*, **12**, 1221–1254, doi:10.1175/2011JHM1380.1.

——, ——, and R. K. Vinukollu, 2012: A global intercomparison of modeled and observed land–atmosphere coupling. *J. Hydrometeor.*, **13**, 749–784, doi:10.1175/JHM-D-11-0119.1.

Findell, K. L., and E. B. Eltahir, 2003a: Atmospheric controls on soil moisture–boundary layer interactions. Part I: Framework development. *J. Hydrometeor.*, **4**, 552–569, doi:10.1175/1525-7541(2003)004<0552:ACOSML>2.0.CO;2.

——, and ——, 2003b: Atmospheric controls on soil moisture–boundary layer interactions. Part II: Feedbacks within the continental United States. *J. Hydrometeor.*, **4**, 570–583, doi:10.1175/1525-7541(2003)004<0570:ACOSML>2.0.CO;2.

——, P. Gentine, B. R. Lintner, and C. Kerr, 2011: Probability of afternoon precipitation in eastern United States and Mexico enhanced by high evaporation. *Nat. Geosci.*, **4**, 434–439, doi:10.1038/ngeo1174.

Fritsch, J., R. Kane, and C. Chelius, 1986: The contribution of mesoscale convective weather systems to the warm-season precipitation in the United States. *J. Climate Appl. Meteor.*, **25**, 1333–1345, doi:10.1175/1520-0450(1986)025<1333:TCOMCW>2.0.CO;2.

Gentine, P., A. A. M. Holtslag, F. D'Andrea, and M. Ek, 2013: Surface and atmospheric controls on the onset of moist convection over land. *J. Hydrometeor.*, **14**, 1443–1462, doi:10.1175/JHM-D-12-0137.1.

Guo, Z., and Coauthors, 2006: GLACE: The Global Land–Atmosphere Coupling Experiment. Part II: Analysis. *J. Hydrometeor.*, **7**, 611–625, doi:10.1175/JHM511.1.

——, P. A. Dirmeyer, and T. DelSole, 2011: Land surface impacts on subseasonal and seasonal predictability. *Geophys. Res. Lett.*, **38**, L24812, doi:10.1029/2011GL049945.

Hohenegger, C., P. Brockhaus, C. S. Bretherton, and C. Schaer, 2009: The soil moisture–precipitation feedback in simulations with explicit and parameterized convection. *J. Climate*, **22**, 5003–5020, doi:10.1175/2009JCLI2604.1.

Huang, H.-Y., and S. A. Margulis, 2011: Investigating the impact of soil moisture and atmospheric stability on cloud development and distribution using a coupled large-eddy simulation and land surface model. *J. Hydrometeor.*, **12**, 787–804, doi:10.1175/2011JHM1315.1.

Juang, J.-Y., A. Porporato, P. C. Stoy, M. S. Siqueira, A. C. Oishi, M. Detto, H.-S. Kim, and G. G. Katul, 2007: Hydrologic and atmospheric controls on initiation of convective precipitation events. *Water Resour. Res.*, **43**, W03421, doi:10.1029/2006WR004954.

Koster, R. D., and Coauthors, 2006: GLACE: The Global Land–Atmosphere Coupling Experiment. Part I: Overview. *J. Hydrometeor.*, **7**, 590–610, doi:10.1175/JHM510.1.

——, S. D. Schubert, and M. J. Suarez, 2009: Analyzing the concurrence of meteorological droughts and warm periods, with implications for the determination of evaporative regime. *J. Climate*, **22**, 3331–3341, doi:10.1175/2008JCLI2718.1.

——, and Coauthors, 2011: The second phase of the Global Land–Atmosphere Coupling Experiment: Soil moisture contributions to subseasonal forecast skill. *J. Hydrometeor.*, **12**, 805–822, doi:10.1175/2011JHM1365.1.

Liu, D., G. Wang, R. Mei, Z. Yu, and H. Gu, 2014: Diagnosing the strength of land–atmosphere coupling at subseasonal to seasonal time scales in Asia. *J. Hydrometeor.*, **15**, 320–339, doi:10.1175/JHM-D-13-0104.1.

Mei, R., and G. Wang, 2012: Summer land–atmosphere coupling strength in the United States: Comparison among observations, reanalysis data, and numerical models. *J. Hydrometeor.*, **13**, 1010–1022, doi:10.1175/JHM-D-11-075.1.

Mesinger, F., and Coauthors, 2006: North American Regional Reanalysis. *Bull. Amer. Meteor. Soc.*, **87**, 343–360, doi:10.1175/BAMS-87-3-343.

Moncrieff, M. W., D. E. Waliser, M. J. Miller, M. A. Shapiro, G. R. Asrar, and J. Caughey, 2012: Multiscale convective organization and the YOTC virtual global field campaign. *Bull. Amer. Meteor. Soc.*, **93**, 1171–1187, doi:10.1175/BAMS-D-11-00233.1.

Nigam, S., and A. Ruiz-Barradas, 2006: Seasonal hydroclimate variability over North America in global and regional reanalyses and AMIP simulations: Varied representation. *J. Climate*, **19**, 815–837, doi:10.1175/JCLI3635.1.

Ruiz-Barradas, A., and S. Nigam, 2013: Atmosphere–land surface interactions over the Southern Great Plains: Characterization from pentad analysis of DOE ARM field observations and NARR. *J. Climate*, **26**, 875–886, doi:10.1175/JCLI-D-11-00380.1.

Santanello, J. A., C. D. Peters-Lidard, and S. V. Kumar, 2011: Diagnosing the sensitivity of local land–atmosphere coupling via the soil moisture–boundary layer interaction. *J. Hydrometeor.*, **12**, 766–786, doi:10.1175/JHM-D-10-05014.1.

——, ——, A. Kennedy, and S. V. Kumar, 2013: Diagnosing the nature of land–atmosphere coupling: A case study of dry/wet extremes in the U.S. southern Great Plains. *J. Hydrometeor.*, **14**, 3–24, doi:10.1175/JHM-D-12-023.1.

Seneviratne, S. I., T. Corti, E. L. Davin, M. Hirschi, E. B. Jaeger, I. Lehner, B. Orlowsky, and A. J. Teuling, 2010: Investigating soil moisture–climate interactions in a changing climate: A review. *Earth-Sci. Rev.*, **99**, 125–161, doi:10.1016/j.earscirev.2010.02.004.

Tawfik, A. B., and P. A. Dirmeyer, 2014: A process-based framework for quantifying the atmospheric preconditioning of surface-triggered convection. *Geophys. Res. Lett.*, **41**, 173–178, doi:10.1002/2013GL057984.

——, ——, and J. A. Santanello, 2015: The heated condensation framework. Part I: Description and southern Great Plains case study. *J. Hydrometeor.*, **16**, 1929–1945, doi:10.1175/JHM-D-14-0117.1.

Taylor, C. M., R. A. M. de Jeu, F. Guichard, P. P. Harris, and W. A. Dorigo, 2012: Afternoon rain more likely over drier soils. *Nature*, **489**, 423–426, doi:10.1038/nature11377.

——, C. E. Birch, D. J. Parker, N. Dixon, F. Guichard, G. Nikulin, and G. M. S. Lister, 2013: Modeling soil moisture–precipitation feedback in the Sahel: Importance of spatial scale versus convective parameterization. *Geophys. Res. Lett.*, **40**, 6213–6218, doi:10.1002/2013GL058511.

van Heerwaarden, C. C., J. V.-G. de Arellano, A. F. Moene, and A. A. M. Holtslag, 2009: Interactions between dry-air entrainment, surface evaporation and convective boundary-layer development. *Quart. J. Roy. Meteor. Soc.*, **135**, 1277–1291, doi:10.1002/qj.431.

Wei, J., and P. A. Dirmeyer, 2012: Dissecting soil moisture–precipitation coupling. *Geophys. Res. Lett.*, **39**, L19711, doi:10.1029/2012GL053038.

Westra, D., G. J. Steeneveld, and A. A. M. Holtslag, 2012: Some observational evidence for dry soils supporting enhanced relative humidity at the convective boundary layer top. *J. Hydrometeor.*, **13**, 1347–1358, doi:10.1175/JHM-D-11-0136.1.